


RESEARCH ARTICLE

Predicting regional tau accumulation with machine learning-based tau-PET and advanced radiomics

Saima Rathore¹  | Ixavier A. Higgins² | Jian Wang² | Ian A. Kennedy² |
 Leonardo Iaccarino² | Samantha C. Burnham² | Michael J. Pontecorvo² |
 Sergey Shcherbinin²

¹Department of Neurology and Department of Biomedical Informatics, Emory University, Atlanta, Georgia, USA

²Eli Lilly and Company, Indianapolis, Indiana, USA

Correspondence

Saima Rathore, Department of Neurology and Department of Biomedical Informatics, Emory University, W226, Health Sciences Research Building I, 1750 Haygood Drive, Atlanta, GA 30322, USA.

Email: saima.rathore@emory.edu

Funding information

Eli Lilly and Company

Abstract

INTRODUCTION: Alzheimer's disease is partially characterized by the progressive accumulation of aggregated tau-containing neurofibrillary tangles. Although the association between accumulated tau, neurodegeneration, and cognitive decline is critical for disease understanding and clinical trial design, we still lack robust tools to predict individualized trajectories of tau accumulation. Our objective was to assess whether brain imaging biomarkers of flortaucipir-positron emission tomography (PET), in combination with clinical and genomic measures, could predict future pathological tau accumulation.

METHODS: We quantified the disease profile of participants ($N = 276$) using a comprehensive set of descriptors, including clinical/demographic (age, diagnosis, amyloid status, sex, race, ethnicity), genetic (apolipoprotein E [APOE]- $\epsilon 4$), and flortaucipir-PET imaging measures (regional flortaucipir standardized uptake value ratio [SUVR] and comprehensive radiomic texture features extracted from Automated Anatomical Labeling template regions). We trained an AdaBoost machine learning algorithm in a 2:1 split train-test configuration to derive a prognostic index that (i) stratifies individualized brain regions including global (AD-signature region) and lobar regions (frontal, occipital, parietal, temporal) into stable/slow- and fast-progressors based on future tau accumulation, and (ii) forecasts individualized regional annualized-rate-of-change in flortaucipir-PET SUVR. Further, we developed an adaptive model incorporating flortaucipir-PET measurements from the baseline and intermediate timepoints to predict annualized-rate-of-change.

RESULTS: In binary classification for predicting stable/slow- versus fast-progressors, the area-under-the-receiver-operating-characteristic curve was 0.86 in the AD-signature region and 0.83, 0.82, 0.84, and 0.83 in frontal, occipital, parietal, and temporal regions, respectively. The trained models successfully predicted

This is an open access article under the terms of the [Creative Commons Attribution-NonCommercial-NoDerivs](https://creativecommons.org/licenses/by-nc-nd/4.0/) License, which permits use and distribution in any medium, provided the original work is properly cited, the use is non-commercial and no modifications or adaptations are made.

© 2024 Eli Lilly and Company. Alzheimer's & Dementia: Translational Research & Clinical Interventions published by Wiley Periodicals LLC on behalf of Alzheimer's Association.

annualized-rate-of-change of flortaucipir-PET regional flortaucipir SUVR in AD-signature and lobar regions (Pearson-correlation [R]: AD-signature = 0.73; frontal = 0.73; occipital = 0.71; parietal = 0.70; temporal = 0.69). The models' performance in predicting annualized-rate-of-change slightly increased when imaging features from intermediate timepoints were used in the adaptive setting (R: AD-signature = 0.79; frontal = 0.87; occipital = 0.83; parietal = 0.74; temporal = 0.82).

DISCUSSION: Taken together, our results propose a robust approach to predict future tau accumulation that may improve the ability to enroll, stratify, and gauge efficacy in clinical trial participants.

KEYWORDS

Alzheimer's disease, adaptive prediction, artificial intelligence, flortaucipir, predictive modeling

Highlights

- Machine learning predicts the future rate of tau accumulation in Alzheimer's disease.
- Tau prediction in lobar/global regions benefits from diverse multimodal features.
- This prognostic index can serve as a sensitive tool for patient stratification.

1 | INTRODUCTION

Alzheimer's disease (AD) is biologically defined by the presence of amyloid β ($A\beta$) and 3R:4R tau proteinopathies.¹ Abundant neuroimaging and pathological data suggest that cortical tau colocalizes with cortical atrophy, both temporally and topographically, and predicts future cognitive decline and neurodegeneration among individuals along the AD spectrum.^{2–4} Moreover, recent evidence suggests the appearance of tau in specific cognitive networks leads to domain-specific cognitive impairments.^{5,6} Consequently, tau has surfaced as a viable therapeutic target for disease-modifying treatments.^{7,8}

Flortaucipir 18F-positron emission tomography (PET) imaging enables the quantification of accumulation of the tau neurofibrillary tangles. This imaging technique serves as a biological definition of AD,⁹ based on the National Institute of Aging-Alzheimer's Association¹⁰ core clinical criteria for possible or probable AD, making it crucial for clinical practice to address the fundamental challenge of predicting tau progression. A reliable prognosis holds significant value for both patients and physicians. Moreover, recognizing the significance of distinct sub-domains associated with various brain regions,^{5,6,11} regional prognosis becomes even more critical. Additionally, the presence of tau pathology serves as a pivotal biomarker in trials, as highlighted in several interventional clinical trials of AD.^{12–14}

Multiple recent studies have identified variables such as age, sex, education, apolipoprotein E (APOE)- $\epsilon 4$ genotype, BIN1 risk allele, cognitive tests, and florbetapir 18F-PET standardized uptake value ratio (SUVR) that are generally available in research settings and are prognostic indicators of the future rates of tau accumulation at different clinical stages of AD.^{15–19} For example, younger age, APOE- $\epsilon 4$ carrier status, and better cognition at baseline independently predicted higher tau accumulation rates in cognitively impaired individuals.¹⁵ An

ongoing challenge is to determine which biomarkers provide the most robust and accurate predictions.

Multiple model-based²⁰ and machine learning-based methods^{21,22} have been proposed to predict individual variability in the pattern of tau accumulation, which could substantially impact clinical trials. Model-based approaches have shown that tau spreading patterns are, to a high degree, explained by the functional connectivity patterns of epicenters in which tau potentially emerges first.²⁰ Other methods using machine learning apply learning models to imaging, genetic, and clinical markers to predict individual variability in the pattern of tau accumulation.²¹ However, the majority of published studies, focus on non-tau biomarkers to predict individualized rate of tau accumulation²¹ or on regional tau measurements from tau-PET to determine the pattern of tau accumulation.^{20,22}

We hypothesize that the rate of tau accumulation has an associated imaging phenotype, which can be predicted by imaging, clinical, and genetic measures. By integrating and analyzing the comprehensive set of imaging, clinical, and genetic data (APOE- $\epsilon 4$ carrier status), we aim to leverage the potential of machine learning and pattern analysis methods to predict the individualized future tau accumulation in the composite AD-signature region,²³ as well as in the four lobar regions of the brain. Unlike traditional methodologies that rely solely on regional tau-PET measurements, we perform a comprehensive profiling of tau across all brain regions using radiomic texture features, thus enhancing our modeling capabilities. Furthermore, we incorporate data from both observational and interventional clinical trials. Our methodology also distinguishes itself by introducing an adaptive predictive approach, leveraging the spatially and temporally rich information derived from baseline and intermediate follow-up tau-PET data. These methods allow us to extract subtle yet distinctive imaging phenotypes that may not be apparent when examining one or a

few imaging variables simultaneously. We tested our predictive models using a dataset that included individuals across the cognitive spectrum ($N = 276$), primarily focusing on symptomatic A β -positive (A β +) participants.

2 | MATERIALS AND METHODS

2.1 | Study participants

We used genomic, clinical, and imaging (florbetapir and flortaucipir) data of 276 participants enrolled in either observational flortaucipir development studies (18F-AV-1451-A05: NCT02016560²⁴) or belonging to the placebo group in interventional clinical trials (EXPE-DITION3: NCT01900665,²⁵ NAVIGATE-AD: NCT02791191,²⁶ and AMARANTH: NCT02245737²⁷). Details on enrollment can be found in [Supplementary Section S1](#). The diagnostic breakdown included 47 cognitively normal (CN) participants, 111 participants having mild cognitive impairment (MCI) due to AD, and 118 participants having AD with mild dementia. Of 276 participants, 184 had available PET images at three different timepoints: baseline and two subsequent follow-ups. The average time between the first and last follow-up visit was 18.8 months.

2.2 | Imaging acquisition and processing

Flortaucipir scans and cognitive assessments were collected at baseline and repeated at follow-up visits. For the analysis of flortaucipir data, the baseline and follow-up flortaucipir scans were motion- and time-corrected,^{3,28} followed by summing into a single scan. After a series of pre-processing steps, the summed flortaucipir scans were transformed into the Montreal Neurologic Institute (MNI) atlas space. More detailed methods of image acquisition and processing are described in an earlier study.²⁴

2.3 | Derivation of global and regional annualized-rate-of-change (continuous outcome)

Flortaucipir retention in AD-signature region was summarized for each participant by SUVR. AD-signature is a data-driven target region of interest (ROI) designed to maximize separation between diagnostic groups (A β + AD, A β + MCI vs. dementia, MCI, and CN A β -subjects) using a multiblock barycentric discriminant analysis.^{23,29} AD-signature-weighted neocortical ROI has higher weights in the posterolateral temporal and parietal regions. The cerebellum crus reference region was used as the SUVR denominator, resulting in AD-signature/cerebellum crus SUVR for each participant. In lobar prediction models, we calculated cortical flortaucipir-PET SUVR in frontal, temporal, parietal, and occipital lobes using the Anatomical Atlas Labeling (AAL) brain atlas,³⁰ with the cerebellum crus as the reference region. The annualized-rate-of-change in SUVR for both AD-signature

RESEARCH IN CONTEXT

1. **Systematic review:** Literature was reviewed using traditional sources, including PubMed. Reports have suggested correlations between tau accumulation and individual clinical and genetic factors. Several reports have also indicated that tau accumulation is closely related to non-tau imaging. Relevant citations have been appropriately cited alongside precedent machine learning models informing the development of our methods.
2. **Interpretation:** Integrating multimodal clinical, imaging, and genetic features using machine learning and pattern analysis methods, we developed a powerful prognostic index. The index can stratify individualized brain regions including global and lobar regions into stable/slow- and fast-progressors based on future tau accumulation (area-under-the-receiver-operating-characteristic curve ≥ 0.82) and forecasts individualized regional annualized-rate-of-change in tau (Pearson correlation ≥ 0.69).
3. **Future directions:** Future research is needed to verify that the proposed index can predict future tau accumulation in different populations and whether individualized endpoints defined based on this index better capture differences in tau progression between therapeutic arms and clinical progression.

and lobar regions was quantified by subtracting baseline SUVR from follow-up SUVR and normalizing by the number of years elapsed since baseline. The derived annualized-rate-of-change was then used to train machine learning regression models (Section 2.6).

2.4 | Derivation of stable/slow- and fast-progressor groups at global and regional level (discrete outcome)

We then approached the prediction through an independent classification mechanism. We used Bayesian multivariate clustering with a mixture of multivariate generalized linear mixed models to discover distinct patterns of longitudinal tau accumulation without imposing any prior assumptions on regions or clinical outcomes. This approach integrated regional flortaucipir tau-PET measures from all timepoints. For global clusters, tau-PET SUVR measurements from four brain lobes (occipital, parietal, occipital, frontal) of both hemispheres were included. At the lobar level, regional flortaucipir tau-PET SUVR of the corresponding lobes from both hemispheres were considered. The optimal number of clusters, determined to be two, captured unique tau progression patterns globally and at the lobar level, which were named as stable/slow- and fast-progressor groups in the respective brain lobes. The derived group/cluster information was then used to train machine-learning classification models (Section 2.6).

2.5 | Quantification of imaging features to be used in predictive modeling

We extracted three primary feature groups from each AAL region of each participant's flortaucipir image: (i) intensity-based, (ii) histogram-related, and (iii) textural features. The intensity-based features include first-order statistics (e.g., mean, median, maximum, minimum, standard deviation [SD], skewness, kurtosis) capturing information on the overall intensity distribution profile. Histogram-related features provide additional characteristics, describing the range and distribution of image gray-level intensity levels (SUVr in PET images). Lastly, texture features include an extensive array of indices that portray both local fluctuations and spatial interdependence of image intensities (based on gray-level co-occurrence matrix [GLCM],³¹ gray-level run-length matrix [GLRLM],³² gray-level size-zone matrix [GLSZM],³² neighborhood gray-tone difference matrix [NGTDM]),³³ and local binary patterns³⁴). Histogram- and texture-based features were extracted using the PyRadiomics package.³⁵

2.6 | Statistical analysis and predictive modeling using machine learning

We trained machine learning models to generate separate prognostic indices of future tau accumulation in global (AD-signature) and lobar regions (frontal, temporal, occipital, and parietal). This index was derived from four categories of baseline biomarkers/features: (i) clinical/demographic markers encompassing age, diagnosis, sex, race, and ethnicity; (ii) APOE- ϵ 4 genotype indicating the absence or presence of one or two alleles, coded as 0, 1, and 2; (iii) cortical A β levels assessed through florbetapir-PET, classifying individuals as A β +/ or A β -,³⁶ coded as 1 and 0; and (iv) texture features and the average flortaucipir-PET signal extracted from AAL regions. Each feature was independently normalized to zero mean and unit variance.

AdaBoost machine learning regressors³⁷ were trained on the selected features to predict the individual annualized-rate-of-change in SUVr both in AD-signature and lobar regions using a 2:1 split train-test configuration (i.e., models were trained on two-thirds of the dataset and tested on the remaining one-third). We chose a 2:1 split for its advantages in handling smaller datasets and minority class cases, ensuring ample testing data, better training, balanced representation, and easier model evaluation. Agreement between the observed versus predicted rate of change was assessed using Pearson's correlation coefficient (R). Within the training process, instead of using all input features, we performed feature selection using support vector machine-based forward feature selection (SVM-FFS). Selection of essential features and optimization of the model's parameter was performed on the training dataset using nested five-fold cross-validation.

To further evaluate how accurately machine learning models can predict future tau accumulation, we formulated a classification task by dichotomizing the participants into stable/slow- and fast-progressors using a 66.6-percentile cutoff (Section 2.4). Feature selection was performed using the SVM-FFS method described above, and an AdaBoost

machine learning classifier³⁸ was trained on the selected features using a 2:1 split train-test configuration. A decision tree with a depth of 50 was used as a weak learner, and the number of estimators and learning rate of AdaBoost were found to be 50 and 0.8, respectively, using 5-fold cross-validation. Agreement between observed versus predicted labels (stable/slow- and fast-progressors) was assessed using classification accuracy, specificity, sensitivity, and area-under-the-receiver-operating-characteristic (ROC) curve. Optimal thresholds along the ROC were defined using the Youden index.

The predictive AdaBoost regressors and classifiers underwent training under two distinct configurations: (i) Baseline-visit Predictive Modeling, which exclusively employed imaging features extracted from baseline flortaucipir images, and (ii) Multi-visit Predictive Modeling, which integrated imaging features from both baseline and intermediate timepoints. Due to the absence of complete three-timepoint data for all participants, the evaluation of adaptive predictive models focused on a subset ($n = 184$) of the entire population possessing three available timepoints. Figure 1 shows an overall schematic of the methodology.

3 | RESULTS

3.1 | Study population baseline demographics and disposition

Table 1 presents the baseline characteristics of participants with all longitudinal measurements needed for our analyses. Of the total 276 participants, 59% were A β +, and 47% were APOE- ϵ 4 carriers. In the complete dataset, the mean age was 72.20 (SD 9.06) years. The patient population was randomly allocated to training and test sets at a 2:1 ratio (training set, $n = 184$; test set, $n = 92$). One-way analysis of variance and chi-square tests were applied to evaluate differences between continuous and categorical variables across training and test groups. The patient populations in the training and test sets were not significantly different in terms of age, sex, diagnosis, and APOE- ϵ 4 carrier status, evaluated using a one-way analysis of variance method and chi-square test applied to continuous and categorical variables, respectively. Further details of training and test sets are provided in Table S1.

The distribution of the annualized-rate-of-change in AD-signature and lobar regions is shown in Figure 2 as a function of age, A β status, and clinical diagnosis. Distributions stratified as a function of age, clustering group (stable/slow- and fast-progressors), and clinical diagnosis are provided in Figure S1.

3.2 | Baseline-visit machine learning models predict global and regional annualized-rate-of-change in tau using multimodal baseline data

The baseline-visit regression prediction model showed a strong correlation ($R = 0.73$, $P < 0.0001$, root mean square error [RMSE] = 0.056) between the predicted and observed annualized-rate-of-change in flortaucipir retention in AD-signature region (Figure 3A). After testing whether our additional machine learning models, trained to

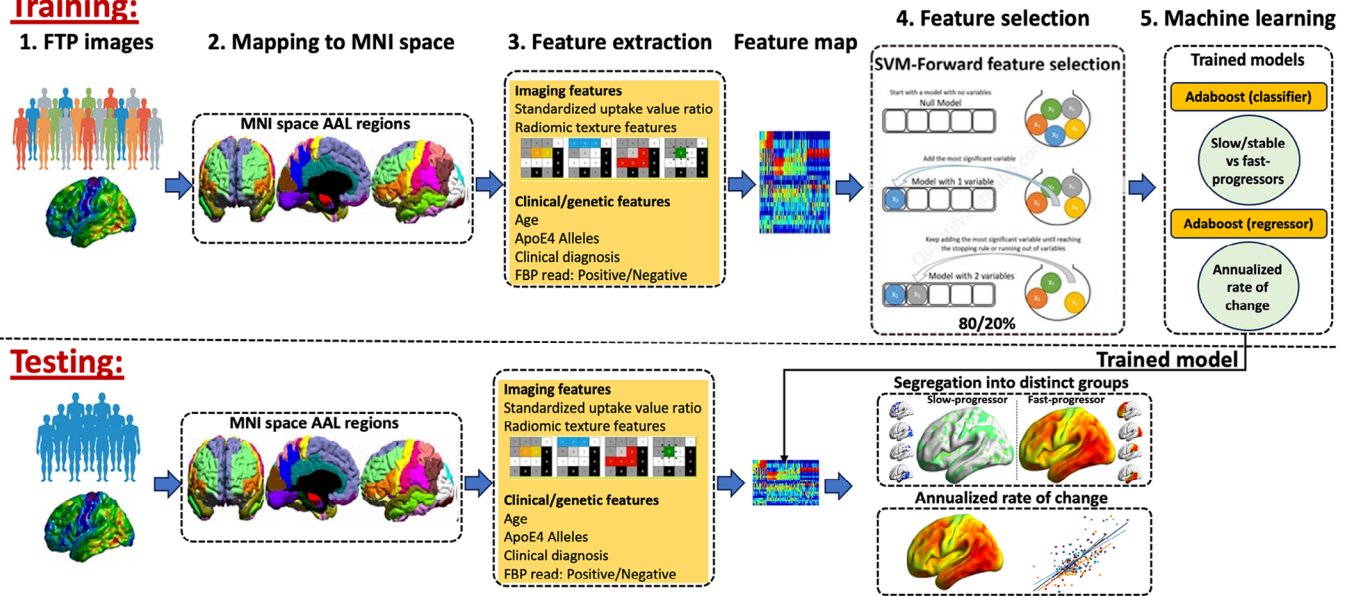
Training:

FIGURE 1 Pipeline for the prediction of tau accumulation. (1) Baseline flortaucipir images processed after applying a series of image processing routines. (2) Mapping of processed flortaucipir images to AAL template in MNI space. (3) Calculation of regional average flortaucipir-PET signal and radiomic texture features from the delineated regions. Clinical measures such as age and diagnosis, genomic descriptor of APOE- ϵ 4, and florbetapir read were also used as features. (4) SVM forward feature selection using 5-fold cross-validation was used to select important features. (5) AdaBoost machine learning regression³⁷ and classification³⁸ models were trained on the selected features using annualized-rate-of-change in flortaucipir-PET SUVR and labels of stable/slow- and fast-progressors calculated at 66.6 percentile as a target variable. AAL, Anatomical Atlas Labeling; APOE, apolipoprotein E; FBP, florbetapir; FTP, flortaucipir; MNI, Montreal Neurologic Institute; PET, positron emission tomography; SUVR, standardized uptake value ratio; SVM, support vector machines.

predict regional retention, could achieve comparable performance, we observed a strong correlation between the predicted and observed annualized-rate-of-change in flortaucipir retention across three lobes (frontal: $R = 0.73$, $P < 0.0001$, $RMSE = 0.051$; occipital: $R = 0.71$, $P < 0.0001$, $RMSE = 0.051$; and parietal: $R = 0.70$, $P < 0.0001$, $RMSE = 0.051$) while correlation in temporal lobe was moderate ($R = 0.69$, $P < 0.0001$, $RMSE = 0.043$). Residuals of the machine learning models (observed annualized-rate-of-change – predicted annualized-rate-of-change) for the complete test set (Figure 3B) and different patient groups based on baseline tau levels (Figure 3C), clinical diagnosis (Figure 3D), and tau progression, where patients are sorted and divided into top 33% and bottom 66% based on annualized-rate-of-change in tau, (Figure 3E) are also shown. The difference between actual versus predicted rate of change in SUVR as a function of tau-PET SUVR at baseline and the average rate of change in SUVR are shown in Figure 3F,G.

3.3 | Baseline-visit machine learning models predict stable/slow- and fast-progressor groups using baseline data

The number of optimal clusters resulting from the data-driven model was two at the global and lobar level. The prevalence of fast-progressors was 67, 97, 99, 107, and 108 in frontal, occipital, parietal, temporal, and AD-signature regions, respectively. Prevalence in the

test dataset was 22, 26, 33, 35, and 36, respectively. The baseline-visit classification model, which included clinical, genetic, and regional tau-PET SUVR measures and texture features, identified the stable/slow- and fast-progressors in the AD-signature region with an accuracy of 82.6% (sensitivity = 80.6%, specificity = 83.9%, area under the curve [AUC] = 0.82, balanced accuracy [BA] = 82.3%). The classification models trained to identify stable/slow- and fast-progressors at the lobar level achieved classification success rates of 83.7% (sensitivity = 90.9%, specificity = 81.4%, AUC = 0.86, BA = 86.2%) in frontal, 82.6% (sensitivity = 84.6%, specificity = 81.8%, AUC = 0.83, BA = 83.2%) in occipital, 80.4% (sensitivity = 78.8%, specificity = 81.4%, AUC = 0.80, BA = 80.1%) in parietal, and 82.6% (sensitivity = 74.3%, specificity = 87.7%, AUC = 0.81, BA = 81.0%) in temporal brain regions (Figure 4A). When evaluated within A β + participants only, BA was similar across almost all regions (AD-signature = 84.3%, frontal = 84.7%, occipital = 82.6%, parietal = 83.8%, temporal = 80.0%). Classification errors were preset in all disease groups, defined based on clinical diagnosis or baseline tau levels (Figure 4B).

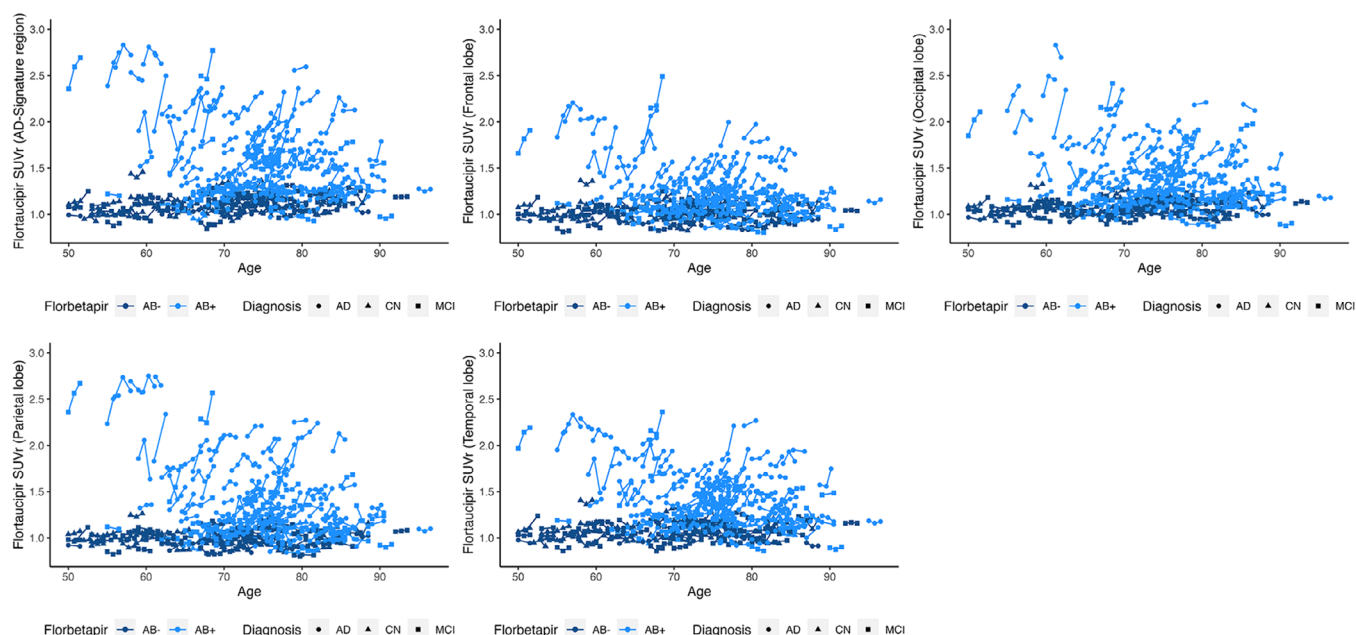
3.4 | Multi-visit models slightly enhance accuracy in predicting tau accumulation compared to baseline-visit models

We trained multi-visit machine learning models to utilize the quantitative imaging covariates extracted from flortaucipir tau scans acquired

TABLE 1 Clinical and genetic characteristics of 276 participants included in the analysis.

Clinical and genetic characteristics	Complete dataset (N = 276)	18F-AV-1451-A05: NCT02016560 ²⁴ (N = 201)	AMARANTH: NCT02245737 ²⁷ (N = 17)	NAVIGATE-AD: NCT02791191 ²⁶ (N = 9)	EXPEDITION3: NCT01900665 ²⁵ (N = 49)
Age, mean years (SD)	72.20 (9.06)	71.74 (9.65)	71.70 (7.05)	72 (5.07)	74.30 (7.51)
Sex: female, n (%)	124 (44.93)	88 (43.78)	6 (35.29)	2 (22.22)	28 (57.14)
APOE- ϵ 4 status: carriers, n (%)	130 (47.10)	80 (39.80)	10 (58.82)	5 (55.55)	35 (71.42)
Florbetapir read: A β +, n (%)	163 (59.05)	88 (43.78)	17 (100.00)	9 (100.00)	49 (100.00)
	n = 272				n = 45
Race					
Asian, n (%)	9 (3.26)	2 (1.00)	2 (11.76)	1 (11.11)	4 (8.16)
Black/African American, n (%)	17 (6.16)	15 (7.46)	1 (5.88)	0 (0.00)	1 (2.04)
White, n (%)	246 (89.13)	184 (91.54)	14 (82.35)	8 (88.89)	40 (81.63)
Clinical diagnosis					
AD with mild dementia, n (%)	118 (45.28)	50 (24.87)	10 (58.82)	9 (100.00)	49 (100.00)
MCI due to AD, n (%)	111 (37.68)	104 (51.74)	7 (41.17)	0 (0.00)	0 (0.00)
CN, n (%)	47 (17.02)	47 (23.38)	0 (0.00)	0 (0.00)	0 (0.00)

Abbreviations: A β +, amyloid beta positive; AD, Alzheimer's disease; APOE, apolipoprotein E; CN, cognitively normal; MCI, mild cognitive impairment; n, number of participants in the analysis; SD, standard deviation.

**FIGURE 2** Florbetapir-PET SUVR signal in AD-signature region and lobar regions of the brain at baseline and multiple follow-up timepoints for individual participants as a function of age. A β +, amyloid β positive; A β –, amyloid β negative; AD, Alzheimer's disease; CN, cognitively normal; MCI, mild cognitive impairment; PET, positron emission tomography; SUVR, standardized uptake value ratio.

from intermediate timepoints. The multi-visit model obtained a strong correlation ($R = 0.79$, $P < 0.0001$) between the predicted and observed annualized-rate-of-change in florbetapir retention in AD-signature region (Figure S2). Additional machine learning models trained to predict the annualized-rate-of-change in lobar regions also obtained strong correlations (frontal: $R = 0.87$, $P < 0.0001$; occipital: $R = 0.83$,

$P < 0.0001$; parietal: $R = 0.74$, $P < 0.0001$; temporal: $R = 0.82$, $P < 0.0001$). The multi-visit model trained to identify stable/slow- and fast-progressors in AD-signature region showed an accuracy of 90.2% (sensitivity = 83.3%, specificity = 93.0%, AUC = 0.88). The multi-visit models trained to identify stable/slow- and fast-progressors at lobar level provided marginally higher classification accuracy compared to

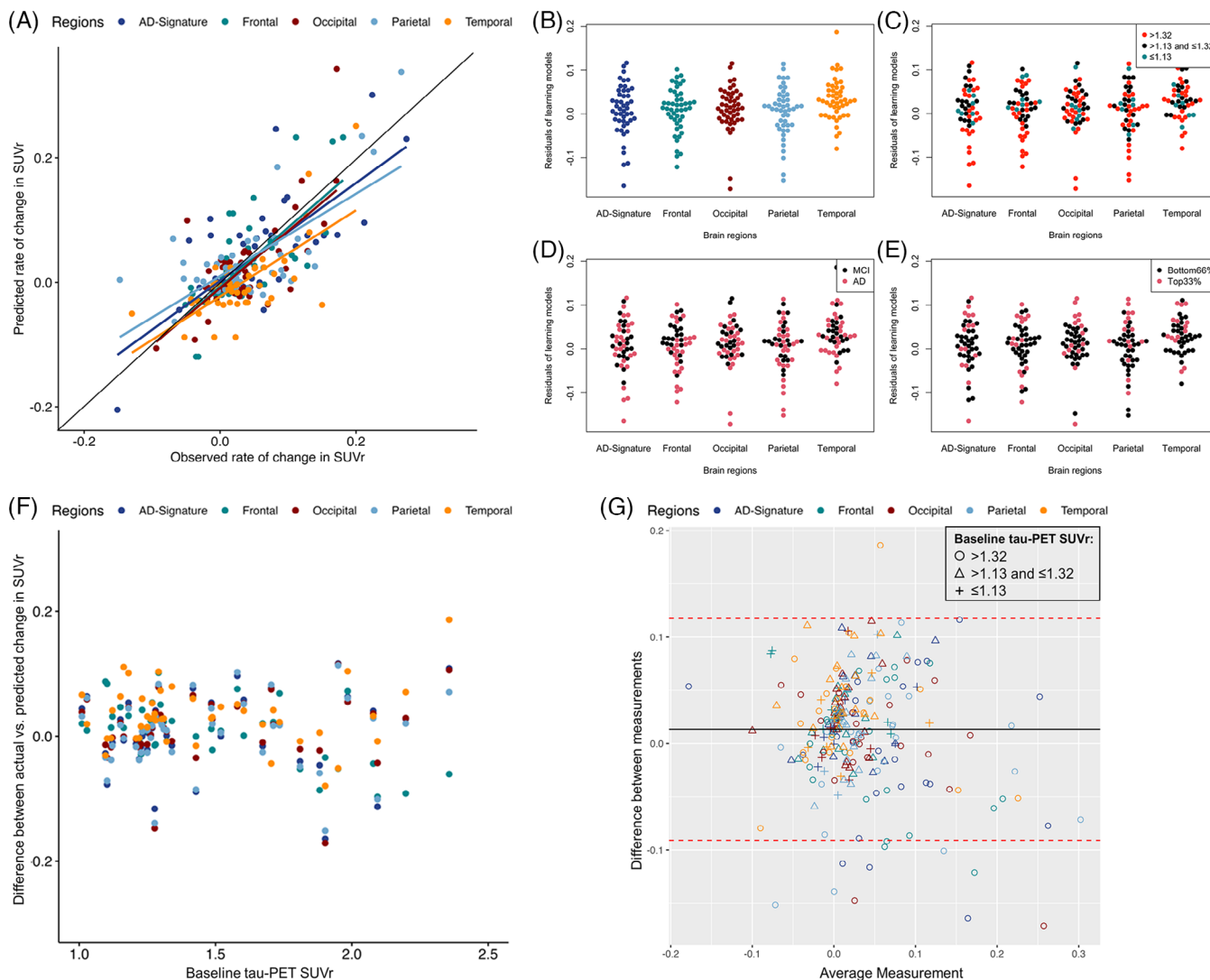


FIGURE 3 (A) Prediction of annualized-rate-of-change in flortaucipir retention in AD-signature and lobar regions using baseline-visit prediction models. Residuals of the machine learning models (actual annualized-rate-of-change – predicted annualized-rate-of-change) are presented for (B) the complete test set and for patient groups categorized by (C) baseline tau, with tercile cutpoints at 1.13 and 1.32 determined from baseline tau-PET SUVR, (D) clinical diagnosis, and (E) annualized-rate-of-change in tau, sorted and divided into top third and bottom two-thirds groups. Difference between actual versus predicted rate of change in SUVR as a function of (F) tau-PET SUVR at baseline (continuous), and (G) average rate of change in SUVR using a Bland-Altman plot. The black solid line shows the mean difference and the dotted red lines represent ± 2 standard deviations from the mean difference. AD, Alzheimer's disease; MCI, mild cognitive impairment; PET, positron emission tomography; SUVR, standardized uptake value ratio.

baseline-visit models (frontal: accuracy = 85.2%, sensitivity = 77.8%, specificity = 88.4%, AUC = 0.83; occipital: accuracy = 86.9%, sensitivity = 81.0%, specificity = 90.0%, AUC = 0.85; parietal: accuracy = 86.9%, sensitivity = 82.4%, specificity = 88.6%, AUC = 0.85; and temporal: accuracy = 86.9%, sensitivity = 84.2%, specificity = 88.1%, AUC = 0.86). Multi-visit models consistently outperformed baseline-visit models, but statistical bootstrapping revealed a nonsignificant difference ($P > 0.05$) between their performances. Baseline-visit models were trained and evaluated using the same dataset as multi-visit models for comparison.

3.5 | Distinct and complementary prognostic information provided by feature categories

To examine the predictive potential of different feature categories, regional flortaucipir-PET, clinical, genomic, and radiomic features were evaluated separately. Flortaucipir-PET SUVR (Figure 5A) in the supramarginal region showed the strongest correlation with annualized-rate-of-change (AD-signature: $R = 0.41$; frontal: $R = 0.51$; temporal: $R = 0.34$; parietal: $R = 0.40$). The leading radiomic features (Figure 5B) primarily indicated spatial homogeneity (coarseness,

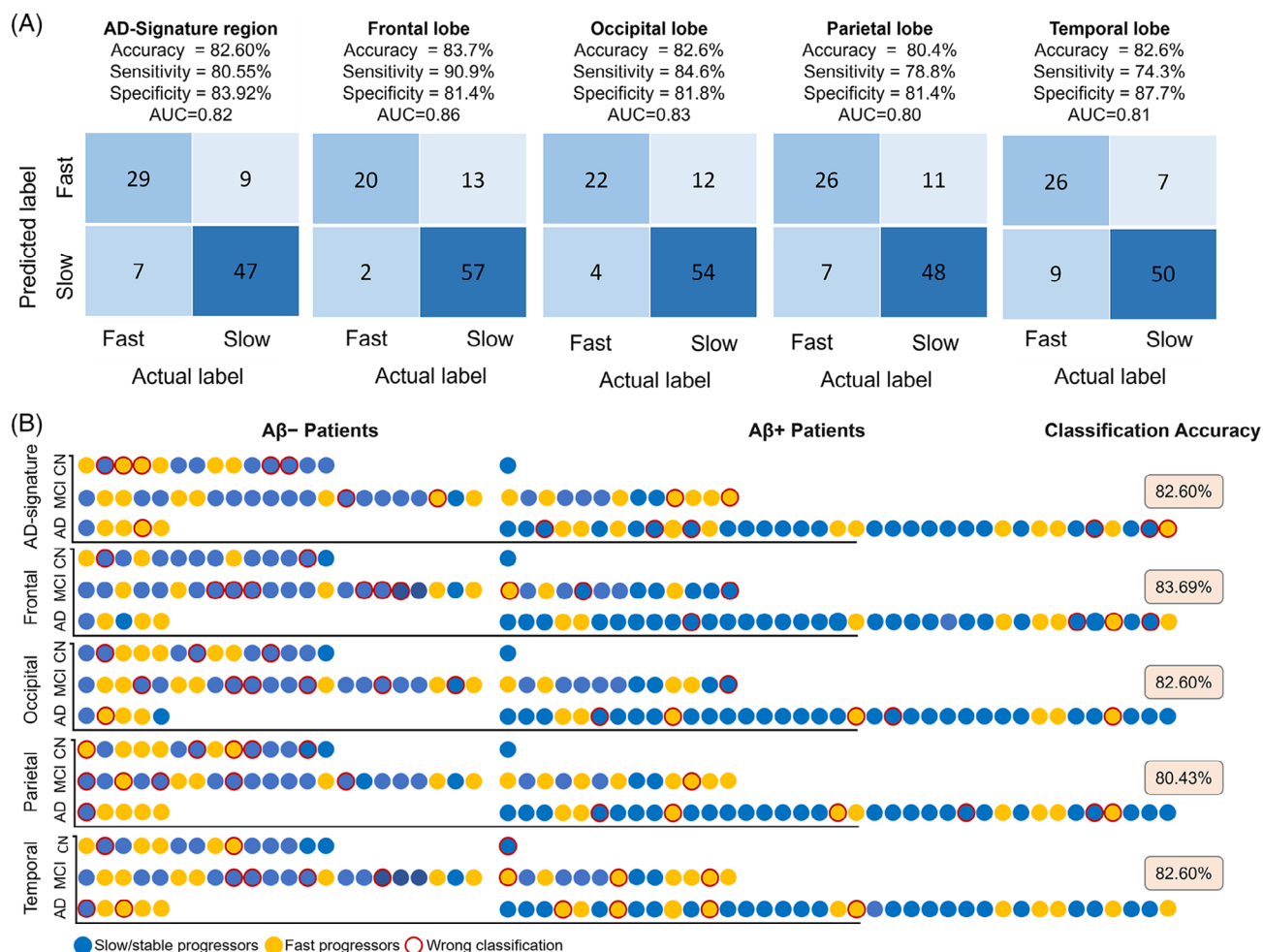


FIGURE 4 (A) Confusion matrices and classification performance of the baseline-visit machine learning models in predicting stable/slow-versus fast-progression in AD-signature and lobar regions. (B) Individual prediction results on the unseen test dataset, categorized by Aβ- and Aβ+ participants and disease group. Participants within each disease group are sorted in ascending order of annualized-rate-of-change to have one-to-one correspondence between the results of different models. Aβ+, amyloid β positive; Aβ-, amyloid β negative; AD, Alzheimer's disease; AUC, area under the curve; CN, cognitively normal; MCI, mild cognitive impairment.

correlation, inverse-difference-normalized) in fusiform, cingulum, middle- and inferior-temporal, and inferior-occipital regions, elevated in participants with higher annualized-rate-of-change. Selected features also reflected spatial heterogeneity (informational measure of correlation [IMC], gray-level non-uniformity [GLNU], small-area high-gray-level emphasis [SAHGLE], and size-zone non-uniformity [SZNU]), mainly in the temporal, fusiform, and cingulum regions, reduced in participants with higher annualized-rate-of-change. Other texture measures predictive of annualized-rate-of-change were related to histogram-based features descriptive of regional gray-levels, mainly skewness and interquartile range in temporal, occipital, and fusiform regions.

Clinical and genetic analysis (Figure 5C) reveals faster tau accumulation in APOE-ε4 carriers versus non-carriers and in Aβ+ versus Aβ- participants across all brain regions. The AD-signature region consistently exhibits the most substantial tau changes, regardless of clinical factors. Clinical impact on tau accumulation is least pronounced in the parietal lobe, sometimes lacking sensitivity to detect effects observed

in other brain regions (baseline flortaucipir-PET SUVR in AD-signature region, $P = 0.061$; diagnosis: CN vs. MCI and CN vs. AD; $P = 0.835$ and $P = 0.819$, respectively). Sex and years of education show no associations with the annualized-rate-of-change in any brain region.

The additive introduction of feature categories resulted in a significant boost to correlation, achieving $R = 0.61$ in regional flortaucipir-PET, $R = 0.66$ in flortaucipir-PET+clinical/genomic, and $R = 0.73$ in flortaucipir-PET+clinical/genomic+radiomic features in the AD-signature region. More detail on distinct and complementary prognostic information of features can be found in [Supplementary Sections S2 and S3](#).

4 | DISCUSSION

Tau tangles are believed to follow a typical pattern of cortical dissemination, as outlined in the Braak staging system.³⁹ However, recent data suggest that tau accumulation patterns vary across

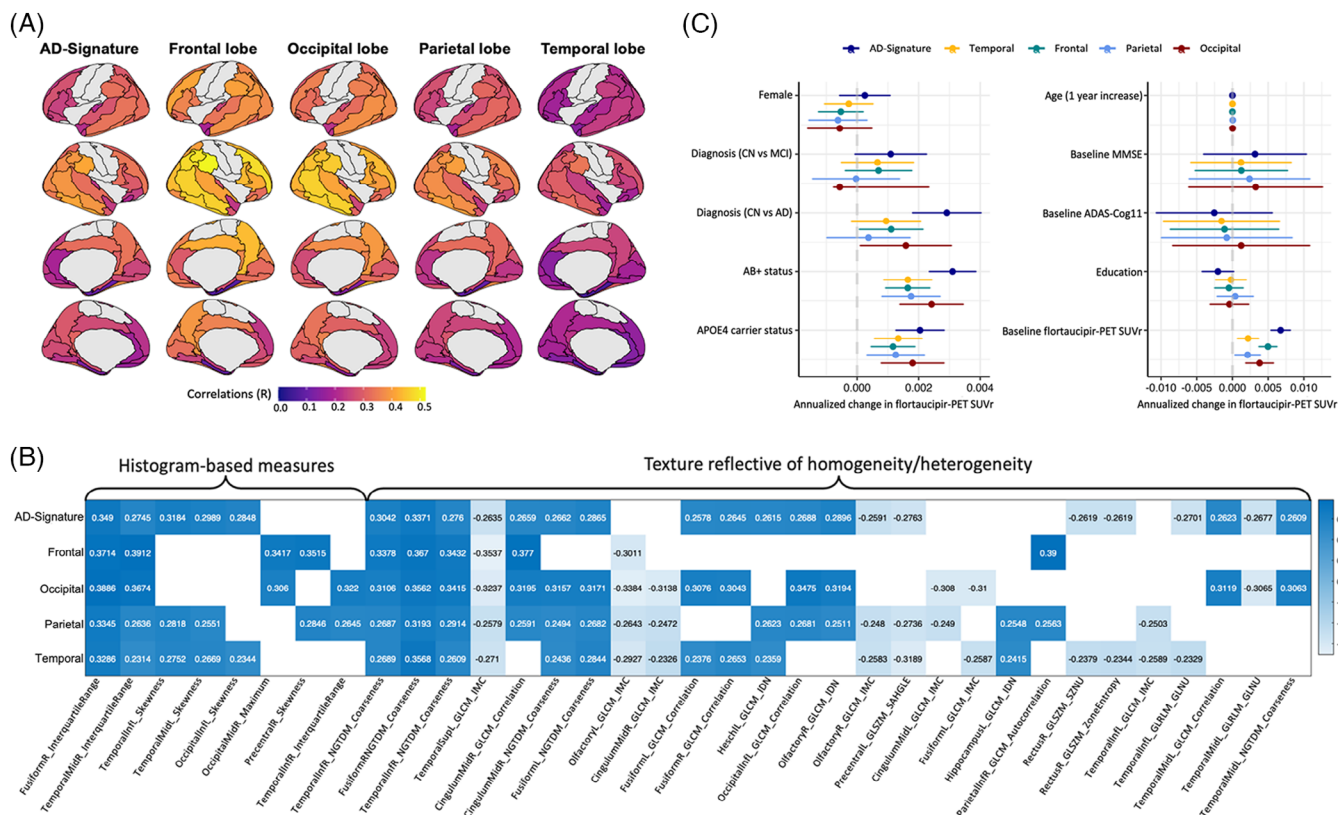


FIGURE 5 Predictive power provided by (A) flortaucipir-PET SUVr, (B) radiomic texture features in individual brain regions, and (C) clinical/genomic features. The left and right sections in (C), respectively, describe feature names as BrainRegion_Feature and BrainRegion_TextureFeatureCategory_FeatureName. AD, Alzheimer's disease; ADAS-Cog11, AD Assessment Scale-Cognitive Subscale; APOE, apolipoprotein E; CN, cognitively normal; FBP, florbetapir; FTP, flortaucipir; GLNU, gray-level non-uniformity; IMC, informational measure of correlation; MCI, mild cognitive impairment; MMSE, Mini-Mental State Examination; PET, positron emission tomography; R, Pearson's correlation coefficient; SAHGLE, small-area high-gray-level emphasis; SUVr, standardized uptake value ratio; SZNU, size-zone non-uniformity.

patients with AD, which could reflect different AD variants that may affect treatment response.⁴⁰ There is a strong need for an analytical predictive tool which provides some quantitative trend of tau progression as the longitudinal data measured in actual studies is variable.

We employed innovative pattern analysis methods that integrated a comprehensive set of features using machine learning to accurately and reproducibly predict annualized-rate-of-change in tau accumulation. Additionally, we developed an adaptive model capable of updating predictions as new measurements become available. The multi-visit model showed a nonsignificant improvement over the baseline-visit model, suggesting that the baseline-visit model provides a relatively robust and accurate prediction of the annualized-rate-of-change. This multimodal prognostic index for tau accumulation is more sensitive for patient stratification than using tau status alone or combined with clinical and genetic markers. The model-training time was 20–24 h, and the inference was 2–3 min on a four-core CPU.

Variables such as age, sex, APOE-ε4 genotype, and tau and amyloid PET are predictive of tau accumulation^{15,16} but have been assessed predominantly utilizing basic regression methodologies in a univariate manner. In contrast, our study used sophisticated radiomic features and machine learning algorithms to discern various phenotypes indica-

tive of future rates of change. A similar model developed by Tosun and coworkers exhibited a balanced classification accuracy of 87% in forecasting stable, fast, and moderate accumulator groups at a global level.²² Our approach exhibited a lower BA of 82%, specifically in the AD-signature region, but predicted the rate of change across all brain lobes with considerable precision and allows adaptive predictions.

Our approach has the potential to inform clinical practice and therapeutic trials in various ways. First, estimation of the expected rate of tau accumulation in the study population can help determine trial duration, sample size, and statistical power. Second, prediction can enable a comprehensive understanding of natural tau progression in the placebo arm, which can help clinicians better anticipate disease trajectory and plan appropriate management strategies. Third, comparing the predicted rate of tau accumulation to the observed rate during treatment, can help evaluate the meaningfulness of the data collected in early phase clinical trials with a limited sample size. Additionally, personalized therapy plans based on an individual's predicted tau accumulation rate might be considered. Finally, our approach can enrich patient populations in terms of tau accumulation and aid stratification by selecting more homogeneous patient subgroups in clinical trials. An example of the potential benefits of our approach in patient stratification is provided in [Supplementary Section S4](#).

Although the cognitive decline is typically the primary outcome measure in late-phase clinical trials,^{12,13} there is mounting evidence suggesting a potential future role for biomarkers such as A β and tau. Recent trials in early AD participants have examined the effects of A β -lowering treatment on clinical progression as well as changes in amyloid and tau burden.^{12–14} Given the strong association between tau and cognitive decline,^{24,41–43} reducing future tau accumulation becomes a relevant intervention target and outcome measure.

Automated machine learning enables simultaneous assessment of multiple features, crucial for analyzing large datasets and uncovering complex patterns hidden by simple models. Our comprehensive approach utilized over 1000 features to construct predictive models, essential as no single variable consistently predicts annualized-rate-of-change, particularly in prospective tests. As evidenced by the effect sizes in Figure 5, features show a correlation with higher/lower rates of tau change, and it is only through the integration of multiple features that highly distinctive patterns predictive of future tau emerge. Moreover, the discriminatory features selected by the model indicate that features from multiple regions contribute to the prediction of tau change in each region. This aspect suggests the importance of connectivity between different brain regions as a connectivity-based, patient-specific model for predicting regional flortaucipir-PET changes has been shown to capture tau accumulation.²⁰

In the participants showing a higher annualized-rate-of-change, we noted that Zone Entropy, a measure of the irregularity or complexity of the signal intensity, was reduced in the rectus regions (Figure 5B). We also observed reduced IMC and GLNU, which also reflect the irregularity or complexity of the signal intensity, in the participants showing a higher annualized-rate-of-change. Specifically, reduced IMC was associated with a higher annualized-rate-of-change in temporal and fusiform regions; reduced GLNU was associated with a higher annualized-rate-of-change in the temporal region. This reduction in tissue complexity accompanied an increased uniformity in the occipital and temporal regions, confirmed by the elevated measures of coarseness and correlation in these regions. This increased uniformity and reduced heterogeneity in various brain regions could reflect an overall increase in the homogeneity of the brain. Though not evaluated on flortaucipir images and precisely in the tau prediction framework in previous studies, the texture features of Entropy and Dissimilarity, whose higher values describe heterogeneous spatial intensity distributions, were correlated negatively to A β +.⁴⁴ Conversely, features like Energy, Homogeneity, and Correlation, whose values increase with higher homogeneity of the image intensity, were correlated positively to A β + when measured using florbetapir⁴⁴ or Pittsburgh compound B-PET.⁴⁵ Texture parameters were also markedly different in cortex, hippocampus, and thalamus regions when compared between tau pathology and wild-type mice based on T2-weighted MRI.⁴⁶

Texture features have also shown an association with A β positivity and conversion to AD. Histogram-based index of skewness was highly correlated with participants' A β status and was a strong marker of progression to AD, as it reflected the prevalence of high- and low-intensity voxels in images of A β + and A β - participants, respectively.⁴⁷ The discriminative ability of histogram-based features was also highlighted

earlier based on separate histogram analysis of gray and white matter to distinguish AD participants from healthy controls.⁴⁸ Although we address a slightly different problem, our analysis also found that skewness of the histogram in certain temporal and occipital regions was positively correlated with annualized-rate-of-change. Similarly, the feature of the interquartile range where higher values correspond to higher intensity values in the region correlated positively with higher annualized-rate-of-change.

Among the clinical and genetic features investigated, higher baseline A β level was positively correlated with the annualized-rate-of-change in tau (Figure 5C), suggesting A β deposition may be an essential precursor for the spread of tau beyond the temporal regions. This association was consistent with studies showing that A β + participants had faster tau progression when evaluated longitudinally.¹⁵ Similarly, clinical diagnosis and APOE- ϵ 4 carrier status, as observed in this analysis, previously have been reported to be associated with faster tau accumulation.^{15,24} There is mixed literature on the association between sex and AD, with some studies showing females at higher risk,⁴⁹ whereas others do not.⁵⁰ In our study, sex was not associated with the annualized-rate-of-change. Based on the association between baseline cognitive function and higher tau accumulation rates in our study, we expected that models might select the Mini-Mental State Examination and AD Assessment Scale-Cognitive Subscale as important discriminative features. However, their shared variance with regional tau features already selected by the model likely explains that the models did not detect these. Comorbidities such as diabetes, hypertension, and depression were investigated in 18-F-AV-1451-A05:NCT02016560,²⁴ but were not found to be associated with the rate of change in tau at both the regional and global levels.

In our analysis, we used the Youden index to optimize sensitivity and specificity. The implications of false positives and false negatives vary depending on the application. For example, maximizing sensitivity may be beneficial in trials for higher-dose administration, while maximizing specificity could be advantageous in experimental treatments.

Despite careful design, including multimodal features, automated delineation of ROI, and independent testing, the analysis presented here has limitations. A major limitation is the retrospective, modestly sized dataset. These models are likely to predict trends in similar future populations but have not been trained on data with extremely diverse inclusion/exclusion criteria or broader demographics. As a result, the findings presented here are strongly attributed to this specific patient population. Accurate predictions in other populations may require training on larger, more diverse datasets. Another limitation is the varying definitions of disease groups across different clinical trials. Although the overall assessment of tau prediction includes all patients together, the performance in different disease groups should be interpreted with caution. Moreover, we used all participants enrolled according to the clinical trial criteria and did not apply any additional restrictions to address co-pathologies. Application of our methods to prospective, longer-term, and larger datasets is needed for further validation and to translate our findings into clinical practice. On the methodological front, there were some cases where the prediction error was about 100% of the observed rate. In the future, we

aim to examine the individual characteristics of these patients to determine contributing factors and refine the modeling approach. We will also seek to evaluate whether individualized endpoints better capture differences in tau progression between therapeutic arms and clinical progression. Another promising direction would be to use deep learning on flortaucipir and florbetapir images to better predict the annualized-rate-of-change in tau.

ACKNOWLEDGMENTS

This study was funded by Eli Lilly and Company. Erika Wittchen, Laura Mizoue, and Dana Melbourne of Syneos Health provided medical writing and editorial support, funded by Eli Lilly and Company.

CONFLICT OF INTEREST STATEMENT

Saima Rathore was affiliated with Eli Lilly and Company at the time of the study and is currently affiliated with Emory University. Ixavier A. Higgins, Jian Wang, Ian A. Kennedy, Leonardo Iaccarino, Samantha C. Burnham, Michael J. Pontecorvo, and Sergey Shcherbinin are employees and shareholders of Eli Lilly and Company. Author disclosures are available in the [Supporting information](#).

CONSENT STATEMENT

This study used data from multiple interventional and observational trials. All trials were conducted in compliance with the Declaration of Helsinki and the International Conference on Harmonization guideline on good clinical practice (World Medical Association, 1997). All patients provided written informed consent to participate in the trials.

ORCID

Saima Rathore  <https://orcid.org/0000-0003-4752-2298>

REFERENCES

- Hyman BT, Phelps CH, Beach TG, et al. National Institute on Aging-Alzheimer's Association guidelines for the neuropathologic assessment of Alzheimer's disease. *Alzheimers Dement*. 2012;8(1):1-13.
- Gordon BA, McCullough A, Mishra S, et al. Cross-sectional and longitudinal atrophy is preferentially associated with tau rather than amyloid β positron emission tomography pathology. *Alzheimers Dement (Amst)*. 2018;10:245-252.
- Pontecorvo MJ, Devous MD, Sr., Navitsky M, et al. Relationships between flortaucipir PET tau binding and amyloid burden, clinical diagnosis, age and cognition. *Brain*. 2017;140(3):748-763.
- La Joie R, Visani AV, Baker SL, et al. Prospective longitudinal atrophy in Alzheimer's disease correlates with the intensity and topography of baseline tau-PET. *Sci Transl Med*. 2020;12(524):eaau5732.
- Bejanin A, Schonhaut DR, La Joie R, et al. Tau pathology and neurodegeneration contribute to cognitive impairment in Alzheimer's disease. *Brain*. 2017;140(12):3286-3300.
- Tanner JA, Iaccarino L, Edwards L, et al. Amyloid, tau and metabolic PET correlates of cognition in early and late-onset Alzheimer's disease. *Brain*. 2022;145(12):4489-4505.
- Jadhav S, Avila J, Schöll M, et al. A walk through tau therapeutic strategies. *Acta Neuropathol Commun*. 2019;7(1):22.
- Cummings J, Blennow K, Johnson K, et al. Anti-tau trials for Alzheimer's disease: a report from the EU/US/CTAD task force. *J Prev Alzheimers Dis*. 2019;6(3):157-163.
- Jack CR, Jr., Bennett DA, Blennow K, et al. NIA-AA research framework: toward a biological definition of Alzheimer's disease. *Alzheimers Dement*. 2018;14(4):535-562.
- McKhann GM, Knopman DS, Chertkow H, et al. The diagnosis of dementia due to Alzheimer's disease: recommendations from the National Institute on Aging-Alzheimer's Association workgroups on diagnostic guidelines for Alzheimer's disease. *Alzheimers Dement*. 2011;7(3):263-269.
- Rathore S, Tronchin G, Higgins IA, et al. Distinct associations between tau-PET and cognitive impairment across brain regions and cognitive domains in Alzheimer's disease. *Alzheimers Dement*. 2023;19(Suppl 14):e078345.
- Mintun MA, Lo AC, Duggan Evans C, et al. Donanemab in early Alzheimer's disease. *N Engl J Med*. 2021;384(18):1691-1704.
- van Dyck CH, Swanson CJ, Aisen P, et al. Lecanemab in early Alzheimer's disease. *N Engl J Med*. 2023;388(1):9-21.
- Sims JR, Zimmer JA, Evans CD, et al. Donanemab in early symptomatic Alzheimer disease: the TRAILBLAZER-ALZ 2 randomized clinical trial. *JAMA*. 2023;330(6):512-527.
- Jack CR, Wiste HJ, Weigand SD, et al. Predicting future rates of tau accumulation on PET. *Brain*. 2020;143(10):3136-3150.
- Leuzy A, Smith R, Cullen NC, et al. Biomarker-based prediction of longitudinal tau positron emission tomography in Alzheimer disease. *JAMA Neurol*. 2022;79(2):149-158.
- Hooli B, Rathore S, Wang J, et al. To assess mediation effects of BIN1 risk variant rs6733839 and APOE4 on Alzheimer's disease pathology. *Alzheimers Dement*. 2023;19(Suppl 12):e080293.
- Steward A, Biel D, Dewenter A, et al. ApoE4 and connectivity-mediated spreading of tau pathology at lower amyloid levels. *JAMA Neurol*. 2023;80(12):1295-1306.
- Wang J, Rathore S, Morris A, Lu M, Sabourin J, Hooli B. Bayesian network analysis of BIN1 risk allele and other risk factors and biomarkers of Alzheimer's disease. *Alzheimers Dement*. 2023;19(Suppl 12):e080307.
- Franzmeier N, Dewenter A, Frontzkowski L, et al. Patient-centered connectivity-based prediction of tau pathology spread in Alzheimer's disease. *Sci Adv*. 2020;6(48):eabd1327.
- Giorgio J, Jagust WJ, Baker S, et al. A robust and interpretable machine learning approach using multimodal biological data to predict future pathological tau accumulation. *Nat Commun*. 2022;13(1):1887.
- Tosun D, Thropp P, Southekal S, Spottiswoode B, Fahmi R, Alzheimer's Disease Neuroimaging I. Profiling and predicting distinct tau progression patterns: an unsupervised data-driven approach to flortaucipir positron emission tomography. *Alzheimers Dement*. 2023;19(12):5605-5619.
- Devous MD, Joshi AD, Navitsky M, et al. Test-retest reproducibility for the tau PET imaging agent flortaucipir F 18. *J Nucl Med*. 2018;59(6):937-943.
- Pontecorvo MJ, Devous MD, Kennedy I, et al. A multicentre longitudinal study of flortaucipir (18F) in normal ageing, mild cognitive impairment and Alzheimer's disease dementia. *Brain*. 2019;142(6):1723-1735.
- Honig LS, Vellas B, Woodward M, et al. Trial of solanezumab for mild dementia due to Alzheimer's disease. *N Engl J Med*. 2018;378(4):321-330.
- Lo AC, Evans CD, Mancini M, et al. Phase II (NAVIGATE-AD study) results of LY3202626 effects on patients with mild Alzheimer's disease dementia. *J Alzheimers Dis Rep*. 2021;5(1):321-336.
- Wessels AM, Tariot PN, Zimmer JA, et al. Efficacy and safety of lanabecestat for treatment of early and mild Alzheimer disease: the AMARANTH and DAYBREAK-ALZ randomized clinical trials. *JAMA Neurol*. 2020;77(2):199-209.
- Shcherbinin S, Schwarz AJ, Joshi A, et al. Kinetics of the tau PET tracer 18F-AV-1451 (T807) in subjects with normal cognitive

- function, mild cognitive impairment, and Alzheimer disease. *J Nucl Med*. 2016;57(10):1535-1542.
29. Abdi H, Williams LJ, Beaton D, et al. Analysis of regional cerebral blood flow data to discriminate among Alzheimer's disease, frontotemporal dementia, and elderly controls: a multi-block barycentric discriminant analysis (MUBADA) methodology. *J Alzheimers Dis*. 2012;31(Suppl 3(03)):S189-S201.
 30. Tzourio-Mazoyer N, Landeau B, Papathanassiou D, et al. Automated anatomical labeling of activations in SPM using a macroscopic anatomical parcellation of the MNI MRI single-subject brain. *Neuroimage*. 2002;15(1):273-289.
 31. Haralick RM, Shanmugam K, Dinstein I. Textural features for image classification. *IEEE Trans Syst Man Cybern*. 1973;SMC-3(6):610-621.
 32. Galloway MM. Texture analysis using grey level run lengths. *Comput Graph Image Process*. 1975;4(2):172-179.
 33. Amadasun M, King R. Textural features corresponding to textural properties. *IEEE Trans Syst Man Cybern*. 1989;19(5):1264-1274.
 34. Ojala T, Pietikainen M, Maenpaa T. Multiresolution gray-scale and rotation invariant texture classification with local binary patterns. *IEEE Trans Syst Man Cybern*. 2002;24(7):971-987.
 35. van Griethuysen JJM, Fedorov A, Parmar C, et al. Computational radiomics system to decode the radiographic phenotype. *Cancer Res*. 2017;77(21):e104-e107.
 36. Pontecorvo MJ, Arora AK, Devine M, et al. Quantitation of PET signal as an adjunct to visual interpretation of florbetapir imaging. *Eur J Nucl Med Mol Imaging*. 2017;44(5):825-837.
 37. Drucker H, editor. Improving regressors using boosting techniques. The 14th International Conferences on Machine Learning. Morgan Kaufmann Publishers. 1997.
 38. Zhu J, Zou H, Rosset S, Hastie T. Multiclass AdaBoost. *Stat Interface*. 2009;2:349-360.
 39. Braak H, Alafuzoff I, Arzberger T, Kretschmar H, Del Tredici K. Staging of Alzheimer disease-associated neurofibrillary pathology using paraffin sections and immunocytochemistry. *Acta Neuropathol*. 2006;112(4):389-404.
 40. Vogel JW, Young AL, Oxtoby NP, et al. Four distinct trajectories of tau deposition identified in Alzheimer's disease. *Nat Med*. 2021;27(5):871-881.
 41. Lu M, Pontecorvo MJ, Devous MD, Sr., et al. Aggregated tau measured by visual interpretation of flortaucipir positron emission tomography and the associated risk of clinical progression of mild cognitive impairment and Alzheimer disease: results from 2 phase III clinical trials. *JAMA Neurol*. 2021;78(4):445-453.
 42. Ossenkoppele R, Smith R, Mattsson-Carlsson N, et al. Accuracy of tau positron emission tomography as a prognostic marker in preclinical and prodromal Alzheimer disease: a head-to-head comparison against amyloid positron emission tomography and magnetic resonance imaging. *JAMA Neurol*. 2021;78(8):961-971.
 43. Lagarde J, Olivieri P, Tonietto M, et al. Tau-PET imaging predicts cognitive decline and brain atrophy progression in early Alzheimer's disease. *J Neurol Neurosurg Psychiatry*. 2022;93(5):459-467.
 44. Seiffert AP, Gómez-Grande A, Milara E, et al. Texture-based analysis of 18F-labeled amyloid PET brain images. *Appl Sci*. 2021;11(5):1991.
 45. Shokouhi S, McKay JW, Baker SL, et al. Reference tissue normalization in longitudinal (18)F-florbetapir positron emission tomography of late mild cognitive impairment. *Alzheimers Res Ther*. 2016;8:2.
 46. Colgan N, Ganeshan B, Harrison IF, et al. In vivo imaging of tau pathology using magnetic resonance imaging textural analysis. *Front Neurosci*. 2017;11:599.
 47. Ben Bouallègue F, Vauchot F, Mariano-Goulart D, Payoux P. Diagnostic and prognostic value of amyloid PET textural and shape features: comparison with classical semi-quantitative rating in 760 patients from the ADNI-2 database. *Brain Imaging Behav*. 2019;13(1):111-125.
 48. Nemmi F, Saint-Aubert L, Adel D, et al. Insight on AV-45 binding in white and grey matter from histogram analysis: a study on early Alzheimer's disease patients and healthy subjects. *Eur J Nucl Med Mol Imaging*. 2014;41(7):1408-1418.
 49. Andersen K, Launer LJ, Dewey ME, et al. Gender differences in the incidence of AD and vascular dementia: the EURODEM studies. EURODEM Incidence Research Group. *Neurology*. 1999;53(9):1992-1997.
 50. Edland SD, Rocca WA, Petersen RC, Cha RH, Kokmen E. Dementia and Alzheimer disease incidence rates do not vary by sex in Rochester, Minn. *Arch Neurol*. 2002;59(10):1589-1593.

SUPPORTING INFORMATION

Additional supporting information can be found online in the Supporting Information section at the end of this article.

How to cite this article: Rathore S, Higgins IA, Wang J, et al. Predicting regional tau accumulation with machine learning-based tau-PET and advanced radiomics. *Alzheimer's Dement*. 2024;e70005. <https://doi.org/10.1002/trc2.70005>